coatings

MDPI

Article

Preparation of Robust Superhydrophobic Coatings Using Hydrophobic and Tough Micro/Nano Particles

Tianyi Feng [1,*,†], Yifan Liu [2,†], Siyan Ye [3], Liping Sheng [3], Binrui Wu [4,*] and Lingcai Huang [1]

[1] Avic General Huanan Aircraft Industry Co., Ltd., Zhuhai 519040, China; huanglc003@avic.com
[2] School of Civil Engineering and Architecture, Southwest University of Science and Technology, Mianyang 621000, China; liuyifan_evan@163.com
[3] National Local Joint Engineering Laboratory for New Petro-Chemical Materials and Fine Utilization of Resources, College of Chemistry and Chemical Engineering, Hunan Normal University, Changsha 410081, China; yesiyan0813@163.com (S.Y.); sleeping1217@126.com (L.S.)
[4] State Key Laboratory of NBC Protection for Civilian, Beijing 102205, China
* Correspondence: fengty009@avic.com (T.F.); binruiwu@foxmail.com (B.W.)
† These authors contributed equally to this work.

Abstract: Superhydrophobic nanocomposite coatings, prepared using adhesive and fillers, offer advantages including ease of fabrication and suitability for large-scale applications, but compared with other types of artificial superhydrophobic surfaces, poor durability still limits these surfaces from practical applications. The utilization of micro/nanoscale particles with both intrinsic hydrophobicity and robust mechanical properties to prepare coatings should significantly contribute to enhanced durability. Herein, rough and hydrophobic particles with micro/nano hierarchical structures were prepared at first, and robust superhydrophobic surfaces were fabricated using the prepared particles and additional nanoparticles. The initially prepared particles formed a rough framework of the coating, while additional nanoparticles provided inevitable nanoscale structures. A series of mechanical tests were carried out to validate the durability, and the surface with 20 wt.% NPs exhibited the best performance, withstanding 30 tape peeling tests, a 2.47 m sandpaper rubbing test (at a pressure of 5 kPa), the impact of 200 g of grit dropped from a height of 20 cm, and a 2 h acidic immersion. These appealing materials may attract attention for self-cleaning, high-speed water impact resistance, anti-icing, and anti-fouling applications in the coatings industry.

Keywords: superhydrophobic coating; durability; abrasion resistance; waterproofing; corrosion resistance

Citation: Feng, T.; Liu, Y.; Ye, S.; Sheng, L.; Wu, B.; Huang, L. Preparation of Robust Superhydrophobic Coatings Using Hydrophobic and Tough Micro/Nano Particles. *Coatings* **2024**, *14*, 1156. https://doi.org/10.3390/coatings14091156

Academic Editor: Marcella Balordi

Received: 12 August 2024
Revised: 3 September 2024
Accepted: 6 September 2024
Published: 8 September 2024

1. Introduction

Superhydrophobic coatings, inspired by their natural prototypes [1,2], exhibit various superior properties such as water resistance [3–5], corrosion inhibition [6–8], high-speed water impact resistance, ice prevention [9], and self-cleaning [1,10], making them valuable in a multitude of disciplines [11,12]. Generally, the superhydrophobic properties can be characterized as being in the Cassie–Baxter state when the water contact angle (WCA) is greater than 150°, and the sliding angle (SA) is less than 10° [13–15]. When the coating surface exhibits strikingly high hydrophobicity, it displays an impressively strong and profound repulsion to liquid corrosive media [16,17]. This distinctive feature is capable of effectively reducing the contact area between the corrosive medium and the surface, thereby minimizing or completely preventing the penetration of the corrosive medium [18–20]. Therefore, it can further improve the corrosion resistance of the substrate, thus extending the service life of coatings and materials [21–23].

According to the Cassie model [24], when a droplet is positioned on a superhydrophobic surface, the actual contact area between the droplet and the solid surface encompasses the interface between the droplet and air within the groove [25]. The smaller this contact

area, the greater the repulsive force. Therefore, to achieve optimal superhydrophobicity, it is essential to minimize the contact area between the droplet and the solid surface [26,27]. This requires our ability to fabricate structures with unparalleled precision at the micro- or nanoscale level. However, during this process, superhydrophobic surfaces may be compromised and lose their water-repellent properties under low loads, which could result in a diminished or even a complete loss of their hydrophobicity [28,29]. Despite the wide variety and meticulous precision of methods for fabricating superhydrophobic surfaces, there are still significant limitations that persist in their practical applications [30–32]. The poor mechanical stability of superhydrophobic surfaces has emerged as a significant impediment to the development of their applications [33]. Therefore, enhancing the durability of superhydrophobic materials has emerged as a key challenge for their practical application [34–36].

Among all types of superhydrophobic materials, those fabricated by mixing micro/nanoparticles with an adhesive agent, known as superhydrophobic nanocomposite coatings, exhibit many advantages, including simplicity of preparation and their suitability for large-scale construction [37–39]. The recent literature in the domain of superhydrophobic coatings has exhibited considerable advancement in regards to fabrication techniques, focusing on achieving optimum wettable surfaces with enhanced properties. For instance, leveraging catalytic hydrosilation for the synthesis of graphene oxide–magnetite (GO-Fe_3O_4) nanocomposite surfaces has emerged as a distinguished method, offering a bioinspired route to superhydrophobicity, with notable antifouling characteristics. This approach, demonstrated by Selim et al. [39], underscores a novel blending of material chemistry and surface engineering. Furthermore, the utility of a polarity-induced phase separation strategy, highlighted by Ma et al. [40], showcases a facile yet effective path toward the fabrication of self-roughened surfaces for superhydrophobic coatings at a reduced cost and in a simpler manner, marking significant progress in the practical application of superhydrophobic materials. Adding to the repertoire of innovative methods, the chemisorption of low surface energy ligands on high-density polyethylene (HDPE) surfaces utilizing nanodiamond-based coatings, as introduced by Arcot et al. [41], exemplifies an advanced method for ensuring superhydrophobicity, along with improved microbiological food safety, leveraging the robust mechanical and hydrophobic properties of nanostructured materials.

However, the thickness of these coatings is extremely limited, and the adhesion to the substrate must be considered [42,43], causing the durability of such superhydrophobic materials to become a concern. At present, the use of micro/nanoparticles to construct micro and nano secondary structures to achieve superhydrophobic properties is a common method of preparation [44,45]. However, although conventional inorganic particles display high hardness and robust mechanical properties, they typically exhibit non-hydrophilic characteristics [46]. Conversely, organic particles such as polytetrafluoroethylene (PTFE), while exhibiting superior hydrophobicity, often show poor mechanical performance [46]. The incorporation of micro/nano-scale particles with both intrinsic hydrophobicity and robust mechanical properties in the preparation of coatings can significantly contribute to enhanced durability [47–50].

Moreover, given the size of micro/nano particles, although there is considerable research focusing on the preparation of superhydrophobic coatings using different particle sizes [51,52], the impact of the micro/nano particle size and its corresponding concentration on coating durability remains unclear [53]. In particular, the content of nanoparticles has a great impact on coating performance, as nanoparticles are the main components in the construction of nanostructures. When the content is too low, it is difficult for the coating to achieve superhydrophobicity, but when the content is too high, the mechanical properties and durability of the coating are significantly reduced due to the large specific surface area of the nanoparticles and their tendency to agglomerate [54,55]. Therefore, the selection of suitable micro- and nanoparticles to prepare superhydrophobic coatings with good durability remains a challenge [56,57].

In this paper, a two-step process to fabricate superhydrophobic surfaces was conducted, aiming to show the effect of microscale hydrophobic particles and additional nanoscale on the durability of superhydrophobic coatings. Firstly, hydrophobic epoxy resin and alumina nanoparticles were selected as raw materials, and intrinsic hydrophobic particles with different particle sizes and micro- and nanostructures were prepared. Then, on this basis, a series of coatings was prepared by changing the content of additional nanoparticles, using raw materials of hydrophobic epoxy resin and self-made hydrophobic micro-scale particles. The physical and chemical durability of these coatings was then thoroughly tested and analyzed, including their internal and external adhesion, as well as their abrasion resistance, dynamic impact strength, and chemical robustness. In addition, changes in surface morphology before and after the tests were observed by SEM. The findings indicate that the initially prepared particles formed a rough framework, while additional nanoparticles provided inevitable nanoscale structures. The surface with 20 wt.% NPs exhibited the best performance, withstanding 30 tape peeling tests, a 2.47 m sandpaper rubbing test (at a pressure of 5 kPa), the impact of 200 g of grit dropped from a height of 20 cm, and a 2 h acidic immersion. These appealing materials may attract attention for self-cleaning, anti-icing, and anti-fouling applications in the coatings industry.

2. Experimental Section

2.1. Materials and Equipment

The experimental raw materials used in this paper are shown in Table 1.

Table 1. Main experimental materials.

Name	Chemical Formula	Specification/Brand	Manufacturer
Aluminum Oxide	Nano-Al_2O_3	30 nm	Shanghai McLean
Ethyl Alcohol	C_2H_6O	99.9%	Sinopharm Group
Ethyl Acetate	$C_4H_8O_2$	99.9%	Sinopharm Group
Polyether Amine	/	D-230	Shanghai Aladdin
Silane Coupling Agent Kh-560	$C_9H_{19}O_5Si$	97%	Sinopharm Group
Perfluorodecyl Trimethoxysilane	$C_{13}H_{13}F_{17}O_3Si$	97%	Shanghai McLean
Concentrated Hydrochloric Acid	HCl	37.5%	Sinopharm Group
Sodium Hydroxide	NaOH	99%	Sinopharm Group
Epoxy Resin	/	E-51	Yueyang Baling Petrochemical
Diethylenetriamine	$C_4H_{13}N_3$	97%	Sinopharm Group

2.2. Experimental Procedure

2.2.1. Preparation of Abrasion-Resistant Particles with Micro and Nano Structures

A total of 2.59 g of modified epoxy resin E51 and 2.59 g of aluminum trioxide nanoparticles were added to the beaker. Ethanol in amounts of 1 to 1.2 times the mass of the aluminum was added and stirred until the modified epoxy resin and alumina trioxide were well mixed; 0.22 g of the curing agent diethylenetriamine was added, and 100 g of silicone oil (viscosity 500 mPa·s) was added after mixing and stirring until the mixture became homogeneous. The beaker containing the above mixture was cured in an oil bath at 80 °C under mechanical stirring so that the epoxy resin encapsulating the aluminum trioxide formed uniform spheres of varying particle sizes in the silicone oil. The beaker was removed after half an hour of reaction.

The mixture in the beaker was diluted 1:1 with ethyl acetate, by volume ratio, and then poured into the Brinell funnel for filtration to obtain a white filter cake. After washing with ethyl acetate three times and drying, self-made wear-resistant particles were obtained.

2.2.2. Preparation of Superhydrophobic Coating

For the preparation of the substrate, an aluminum plate was used as the coating substrate, which was fully sanded until the surface was frosted and matte; then the surface was washed with ethanol and dried to prepare it for further use.

For the preparation of the resin mixture, a total of 2.38 g of modified epoxy resin and a certain amount of self-made hydrophobic particles, along with 7 g of inorganic nanopowder, were added to ethyl acetate. Then, the mixture was processed with a high-speed shearing machine and an ultrasonic disperse machine to ensure that all the particles and resins were uniformly dispersed. Next, 0.62 g of D-230 (the curing agent) was added and stirred well, then set aside. The rough structure of the superhydrophobic coating is determined by the content of particles incorporated in the coating, so it is crucial to determine the composition ratio that can form the superhydrophobic coating. The results are shown in Table 2.

Table 2. Composition percentage of various self-made particle coatings.

Nanopowder Content (wt.%)	Prepared Hydrophobic Particles	Nano-Al_2O_3	Total Mass of Modified Epoxy Resin and Curing Agent
0	7	0	3.0
10	6.3	0.7	3.0
20	5.6	1.4	3.0
100	0	7.0	3.0

The superhydrophobic coating was fabricated using a drop-coating method. A total of 0.8 mL of the dispersed liquid was dropped onto the surface of the aluminum plate with a dropper, and the aluminum plate was rotated to make the dispersed liquid flow evenly. The aluminum plate was placed into an oven, cured at 80 °C for three hours, and then cooled to room temperature to obtain the specimen.

2.3. Characterization

To determine the micro/nano structure of the particles and the coating surface, the surface morphology of the samples was characterized by scanning electron microscopy.

The contact angle of the coating surface was measured with a contact angle meter. A 5 μL droplet of water was placed on the surface of the coating, and after the droplet was spread and stabilized on the surface of the coating, the angle was photographed and fitted with a contact angle meter. The test was repeated several times for each specimen, and the average value was employed as the contact angle value for that specimen.

The determination of the rolling angle necessitates the establishment of a slanted platform. A total of 10 μL of water droplets was dropped from a height of 1 cm, and if the droplets exhibited a rolling behavior, the platform was deactivated to the point where the droplets no longer rolled on the surface, indicating that the inclination angle of the platform was the rolling angle of the surface.

In this section, the sandpaper abrasion method was used to study the abrasion resistance of the samples. After the sample was placed on a flat table, the sandpaper was attached to the bottom of the weight, and a driving force parallel to the table was exerted on the weight to pull the weight at a speed of 1 m/min.

The tape peeling test and the cross-cut method were used to test the external and internal adhesion capacity of the coating, respectively. The adhesive tape used was 3M VHB 4910, with a viscosity strength of approximately 2600 N/m. A 2 kg weight was rolled over the tape to ensure that the tape was in full contact with the surface, and then the tape was quickly peeled. The process was repeated until the coated surface lost its superhydrophobic properties. The cross-cut method was also applied using 3M VHB 4910 adhesive tape. A total of 6 to 11 cuts were made in the horizontal and vertical directions of the coating, and then the tape was applied; the coating loss was compared to the parameters listed in the ASTM D3359 standard [58].

The specimen was placed on an inclined table with an inclination angle of 45°, and the lower mouth of the funnel was fixed at a certain height from the specimen; the grit was then dropped into the funnel and allowed to fall naturally, and a contact angle test was carried out after each impact until the surface of the coating lost its superhydrophobic properties.

3. Results and Discussion

3.1. Preparation of Hydrophobic Particles with Micro/Nano Structures

According to the limitations of most of the superhydrophobic coatings mentioned in the introduction section, an abrasion-resistant hydrophobic particle with a micro and nano surface structure was synthesized in this paper to realize the protection of the strong micron structure for the nanostructure. The coating was achieved by adding aluminum oxide to hydrophobic epoxy resin, diluting the mixture with solvent, adding curing agent to mix evenly, and then adding silicone oil as a dispersant, stirring evenly to form a uniform oil–water dispersion system so that the epoxy-coated aluminum forms uniform small droplets in the system. A mechanical stirring arm was used to stir the liquid droplets to keep them suspended in the silicone oil and to provide further even dispersion of the droplets during heating and curing. After the reaction is completed, white abrasion-resistant particles can be obtained by pumping and filtering.

In this section, the influence of the inorganic nanoparticle content on the self-made particles was first explored. Four gradient nanoparticle contents of 20 wt.%, 40 wt.%, 50 wt.%, and 60 wt.% were chosen, and other factors were fixed to study the influence of inorganic nanoparticle content on surface structure. The content of 30 wt.%. was not investigated, as it can be observed that the surface changes from smooth to rough, and the shape changes significantly when employing the 40 wt.% to 60 wt.% content. However, the difference between 20 wt.% to 40 wt.% was not clear. Thus, the sample with 50 wt.% of nano-Al_2O_3 was prepared. Then, the impact of mechanical stirring speed on the self-made particles was explored to study the effect of rotating speed on the size and morphology of the particles.

Figure 1 shows the surface morphology of four kinds of particles under the same mechanical stirring speed. As shown in Figure 1, the self-made particles with a nanoparticle content of 20 wt.% are homogeneously spherical, but the surface is smooth and does not have the micro/nano structure required by the scheme. The particles with a nanoparticle content of 40 wt.% are also homogeneously spherical, and the surface microstructure of the particles begins to appear. When the nanoparticle content is 50 wt.%, the nanoparticle displays both a spherical structure and a surface micro/nano structure. When the nanoparticle content was 60 wt.%, the self-made particles could not remain spherical but exhibited a rough micro/nano structure. Considering the surface structure and shape required for superhydrophobicity, particles with 50 wt.% NPs were chosen for additional experiments.

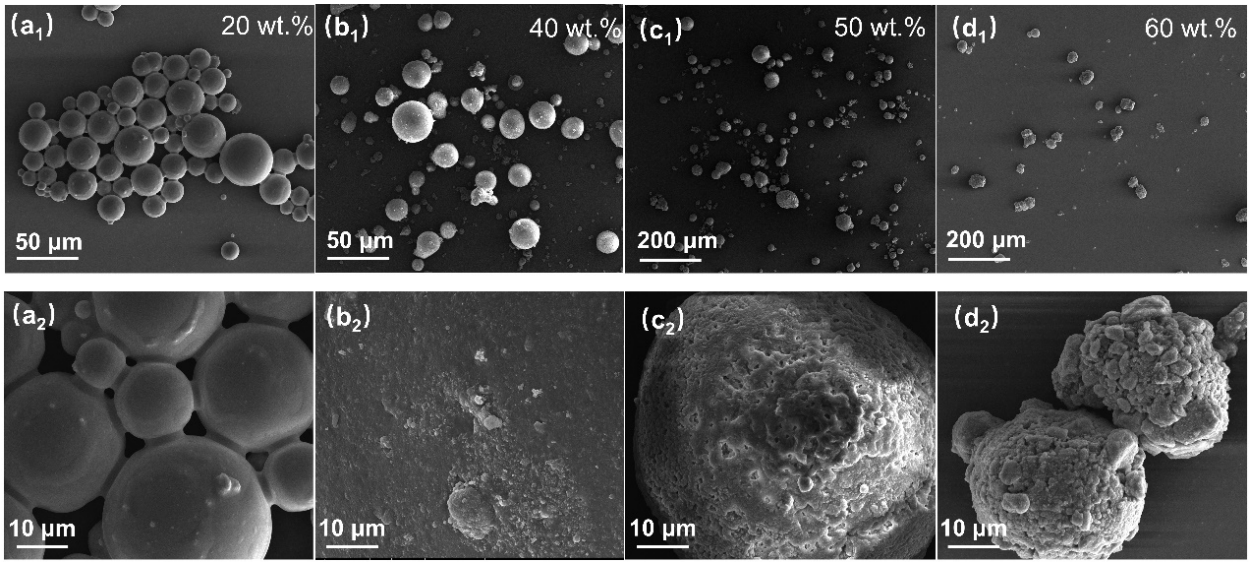

Figure 1. Surface microscopic morphology of particle specimens with different Al_2O_3 nanoparticle contents: (**a1**,**a2**) 20 wt.%; (**b1**,**b2**) 40 wt.%; (**c1**,**c2**) 50 wt.%; (**d1**,**d2**) 60 wt.%.

To further explore the influence of mechanical stirring speed on particle morphology, the mechanical stirring speed was set at 100/200/400/600/800/1000 r/min. The results are shown in Figure 2. According to SEM images, the particles prepared at low rotational speeds would adhere to each other and could not be separated, forming massive and irregular large particles which are not suitable for dispersion, as shown in Figure 2a,b. When the rotational speed reached 400 r/min, the particles began to separate, but they were not regular enough. When the mechanical stirring speed was 600 r/min, the particles formed individual balls that no longer stuck to each other, and the surface of the particles displayed a rough structure. When the speeds reached 800 r/min and 1000 r/min, the sphere became very smooth, but the surface was too smooth, lacking the rough micro/nano structure required for the purposes of this paper.

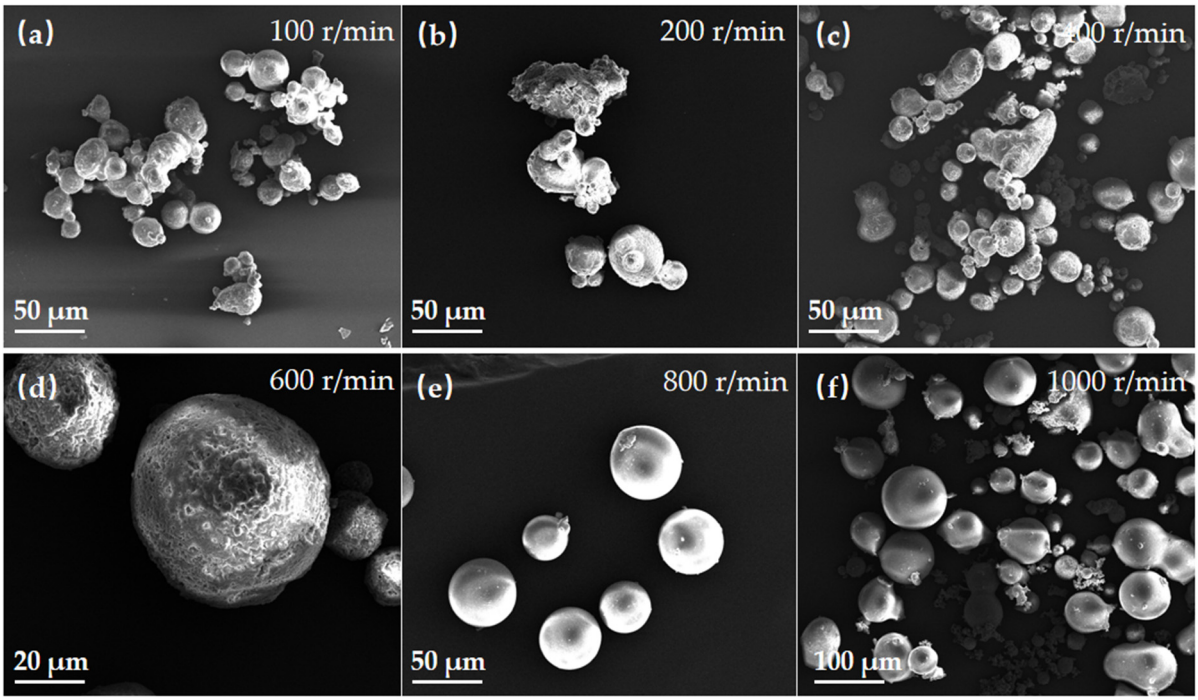

Figure 2. The surface microstructure of samples prepared using different mechanical stirring speeds: (**a**) 100 r/min; (**b**) 200 r/min; (**c**) 400 r/min; (**d**) 600 r/min; (**e**) 800 r/min; (**f**) 1000 r/min.

Furthermore, the particle size distribution of particles obtained using different mechanical stirring speeds was determined according to the mass percentage. The result is obtained by sieving the specimen with different sifters and measuring the mass of each residue. It can be seen from Table 3 that the particle size is inversely proportional to the speed of mechanical mixing, i.e., the greater the speed, the smaller the size of the self-made particles. Thus, the particle prepared using 600 r/min with 50 wt.% NPs was determined for the fabrication of the superhydrophobic coating.

Table 3. Particle size distribution of samples prepared using different mechanical stirring speeds.

Rotate Speed (r/min) / Particle Size (μm)	100	200	400	600	800	1000
<48	0	0.90	0.48	1.60	1.35	2.90
48~106	0.12	5.00	5.00	20.71	51.33	36.03
106~212	3.40	26.67	45.21	74.75	47.05	60.01
212~425	10.00	41.34	46.00	2.70	0.28	1.07
>425	86.45	26.10	3.32	0.25	0	0

3.2. Wettability and Durability of Prepared Coatings

Based on the prepared particles, coatings were prepared using hydrophobic epoxy resin and additional aluminum NPs. Nanoscale roughness is important for constructing and retaining water repellence; thus, the effect of NPs on wettability, as well as the robustness of these prepared coatings, were the main concerns.

Figure 3 shows the wettability of the coating under different nanoparticle ratios. As can be seen in Figure 3, the coating with 0 wt.% of the total mass of the self-made abrasion-resistant particles and inorganic nanoparticles does not exhibit superhydrophobic properties, but the other coatings do display these characteristics. Therefore, in the following work, only the coating durability of the 10 wt.%, 20 wt.%, and 100 wt.% ratios was explored.

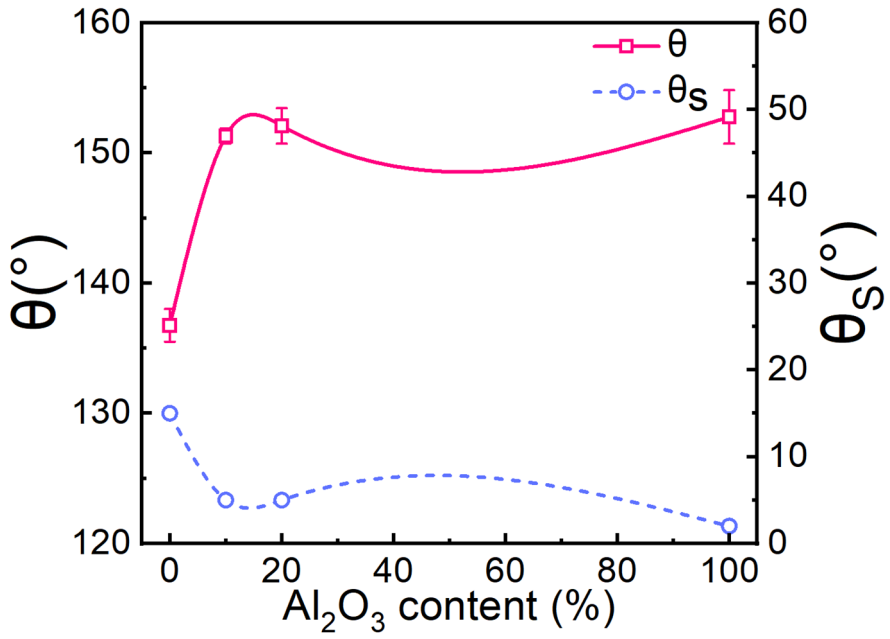

Figure 3. The variation in the surface hydrophobic properties with different nanoparticle contents.

The formation of the superhydrophobic surface is related to surface roughness. Figure 4 shows the SEM image of the coating surface provided by three different components. It can be observed that the coatings consisting of the three different ratios exhibit different microstructures due to their different components. As shown in Figure 4a,b, the surface structure of the coating with an inorganic nanoparticle content of 10 wt.% is more porous than that of the coating with an inorganic nanoparticle content of 20 wt.%, but all of them display micron-scale structures and can form superhydrophobic surfaces. However, the coating with a content of 100 wt.% of inorganic nanoparticles (as shown in Figure 4c) exhibits a smooth surface, with no obvious micron structure.

However, at the nanoscale level, according to the SEM image, it can be seen that the greater the content of inorganic nanoparticles, the more obvious the nanostructure. As shown in Figure 4d–f, the resin acts as a bonding agent. The more inorganic nanoparticles included in the sample, the coarser of the nanoscale structures. The coating with a nanoparticle content of 100 wt.% displays a large number of Al_2O_3 nanoparticles distributed on its surface, a nanosized microporous structure, and superhydrophobic properties. According to the fraction of inorganic nanoparticles in the total mass of all particles, the coatings were labeled as C10, C20, and C100.

Next, the durability of the prepared superhydrophobic coatings was emphasized, and abrasion durability tests, tape peel tests, grid division tests, acid–base immersion tests, and dynamic impact tests were carried out to evaluate the performance of the coatings.

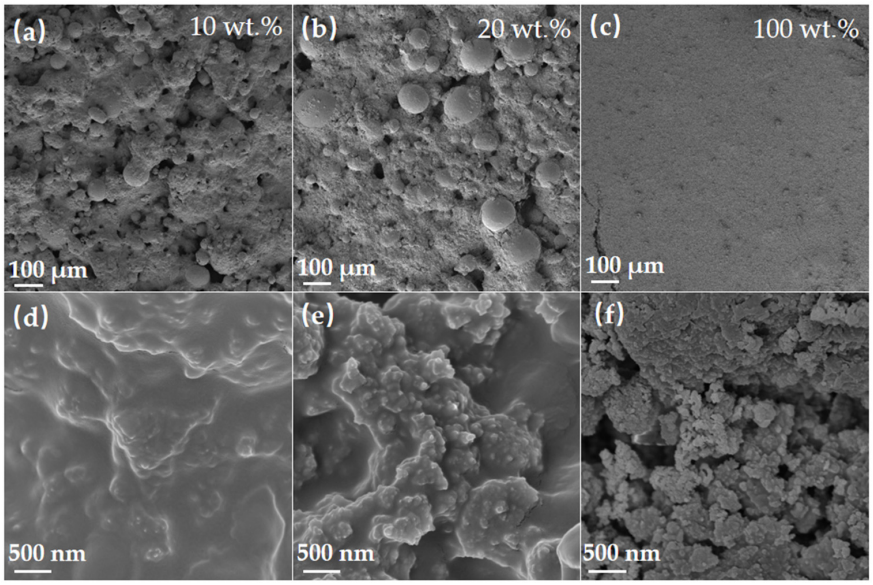

Figure 4. Surface microstructure of coated samples with different Al_2O_3 nanoparticle contents: (**a**,**d**) 10 wt.%; (**b**,**e**) 20 wt.%; (**c**,**f**) 100 wt.%.

The adhesion of the coating can be classified as either external adhesion and internal adhesion. If the adhesion capability is deficient, it is extremely probable that the coating will experience peeling and delamination during its application. Therefore, it becomes imperative to test the adhesive capacity of the coating.

The external adhesion was tested using the cross-cut method, and the three samples were evaluated against the ASTM D3359 standard after testing. As shown in Figure 5, it can be seen that the damage area of the coating with 10 wt.% and 20 wt.% nanoparticles is less than 5%, which is rated 4B in this test. Coatings with a nanoparticle content of 100 wt.% show a damage area greater than 65%, earning them the lowest rating of 0B in this test. The test results show that the addition of wear-resistant particles is beneficial to the external adhesion of the coating, and an excessive amount of NPs is detrimental to the adhesion strength. As C100 exhibits poor adhesion to the substrate, there is no need for further investigation of this sample.

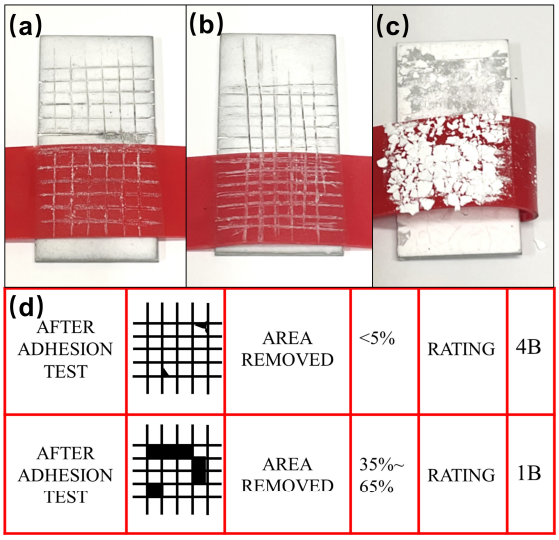

Figure 5. Test results for the coating grid division method: (**a**) 10 wt.%; (**b**) 20 wt.%; (**c**) 100 wt.%; (**d**) damage area and corresponding classification after the test. The black area represents the detached portion after the test, while the white area represents the intact area.

The internal adhesion ability of the tape was further tested, along with the cohesion bonding strength between particles in the coating. The test of the internal adhesion capacity was conducted using the tape-adhesion method, as illustrated in Figure 6, which presents the results of the tape tests using two types of coatings, C10 and C20. According to the test results, as shown in Figure 6a,b, these coatings performed better in terms of internal adhesion capacity, as C10 lost its ability after 25 cycles, and C20 could withstand more than 30 tests, which confirms the role of NPs in retaining superhydrophobicity.

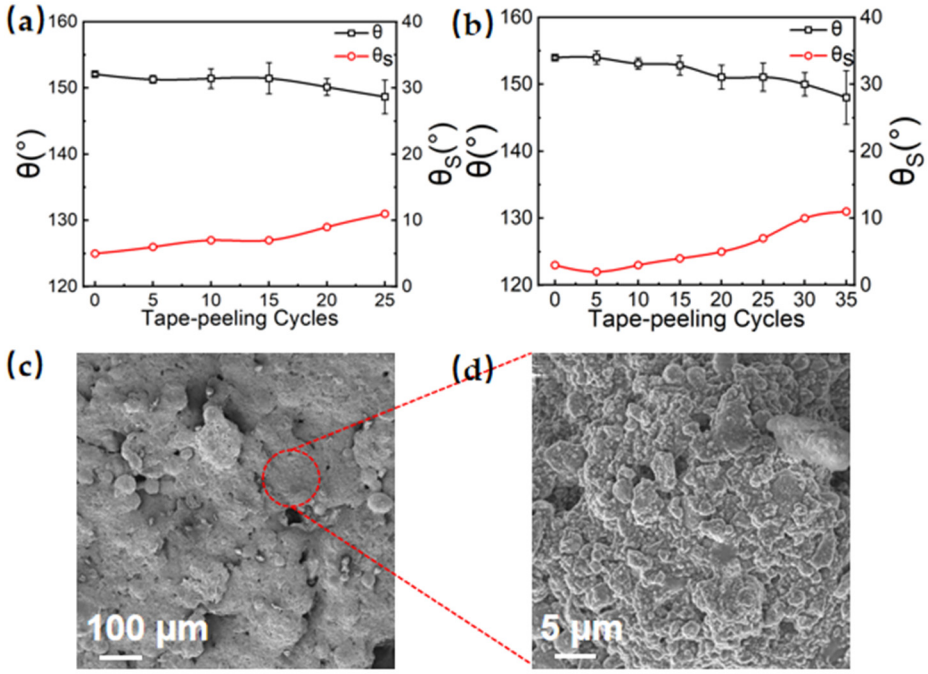

Figure 6. Tape peeling test results for the coating samples: (**a**,**b**) test results for C10 and C20, respectively; (**c**,**d**) surface morphology of the sample after the test.

According to the surface morphology of the tested C20 sample shown in the SEM image in Figure 6c, after 30 cycles of testing, the C20 coating still exhibits a rough surface structure, as initially observed before testing. However, when compared with the pristine sample, the height of the columnar structures on the surface has decreased, and the roughness has also diminished. Particles that were poorly adhered to the epoxy resin have been detached by adhesive tape, resulting in a reduction in the number of self-made particles on the surface. This structural transformation in the C20 coating is attributed to the adhesive tape removing particles and layers that are not strongly bonded to the surface, leaving behind those that are well integrated, thus forming the structures depicted in the figure.

In summary, this section utilized two separate test methods to assess the adhesion capacity of coatings, revealing that the C20 coating yields superior results. The C20 coating exhibits robust resistance to 30 cycles of tape peel testing and earns a grade of 4B in grid division evaluation.

In practical utilization, the coating is prone to certain degradation due to external environmental abrasion. To accurately assess its performance under these conditions, a sandpaper abrasion test was devised. A uniform force was applied to this device, which was then moved at a constant speed across the coated surface. For the abrasion test, both 80 grit and 600 grit sandpapers were utilized to evaluate the durability of the coating against abrasion, with a constant pressure of 5 kPa being applied. Each test involved a sliding distance of 4.5 cm.

As demonstrated in Figure 7, the C10 coating can withstand 20 cycles of abrasion using 80 grit sandpaper and 35 cycles of abrasion using 600 grit sandpaper before losing its superhydrophobic properties. For the C20 coating, its performance is superior, retaining its

superhydrophobic properties after 40 cycles of abrasion with 80 grit sandpaper and 50 cycles with 600 grit sandpaper, with both results superior to those for the C10 coating. This may be attributed to the fact that more nanoparticles can contribute to the maintenance of the nanostructure during abrasion, thereby enhancing the durability of the superhydrophobic properties.

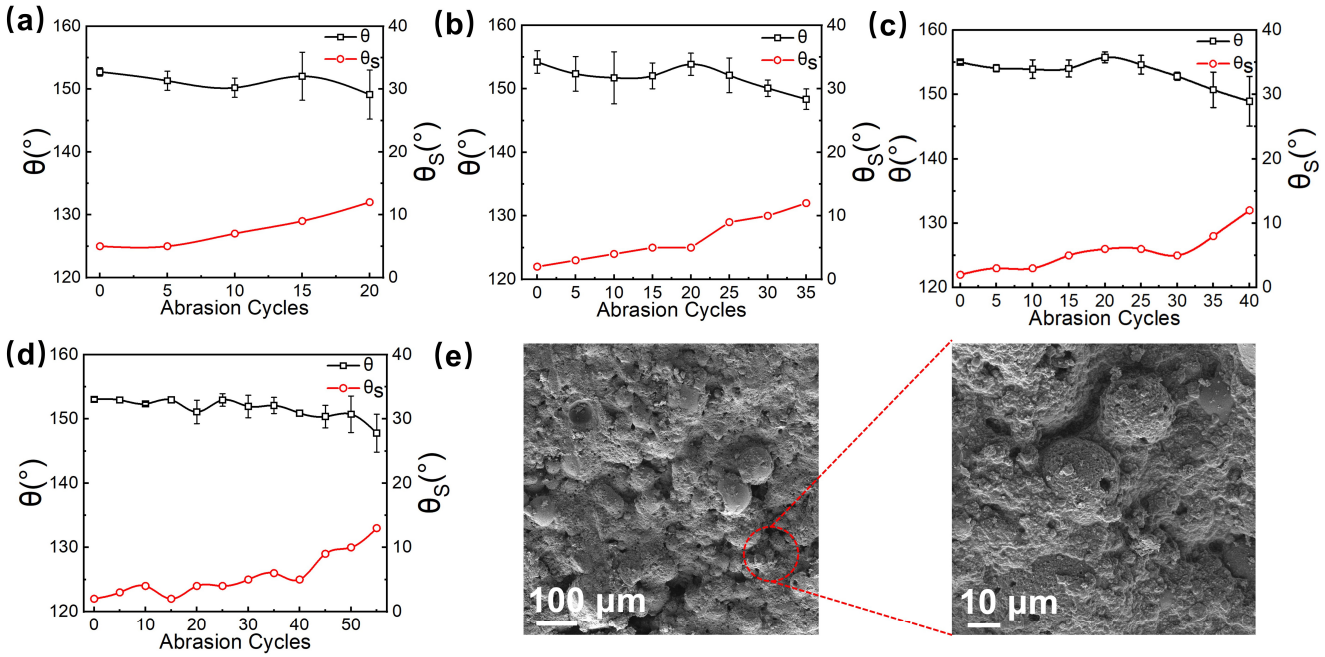

Figure 7. Sandpaper abrasion test results: (**a**,**b**) C10 sample test results for 600 grit and 800 grit sandpaper abrasion, respectively; (**c**,**d**) C20 sample test results for 600 grit and 800 grit sandpaper abrasion, respectively; (**e**) the surface microstructure of the sample after abrasion testing.

Subsequently, the surface morphology of the coating was observed by SEM after the abrasion test, and the results are shown in Figure 7e. Obvious traces of abrasion can be seen on the surface of the C20 coating after the test, and some particles showed the phenomenon of debonding and damage. In addition, the entire surface became significantly smoother than before. However, further magnification of the structure shows that the relatively obvious nanoscale structure can still be observed on the self-made particles. This indicates that the micron particles with larger sizes can protect the nanostructure, to a certain extent, during the abrasion, and the self-made particles prepared in this paper are inherently hydrophobic, which makes them conducive to the retention of the superhydrophobic properties of the coating after the abrasion.

Since the coating will be damaged by solids, such as wind and sand, in the actual environment, the sand impact method is used to simulate the impact of the real environment on the coating. The sand impact test results are shown in Figure 8a,b. The results of the sand impact testing show that the C10 coating can only withstand 150 g of sand impact (50 g per impact), and the C20 coating can withstand 250 g of sand impact in the test. As illustrated in Figure 8c,d, SEM analysis indicates that the structure of the C10 coating has been broken by the impact of sand gravel, resulting in damaged columnar architecture and an abundance of debris. Furthermore, a significant number of micrometer-scale holes emerged on the surface after the roughened structure of the coating was damaged, and essentially, only self-made particles remained on the surface layer; thus, C10 lost its superhydrophobic property. The results for the C20 coating were relatively better compared to those for the C10 sample: the surface structure was still retained, along with a rough structure, but the columnar structure had been damaged, and the structure had become unidentifiable.

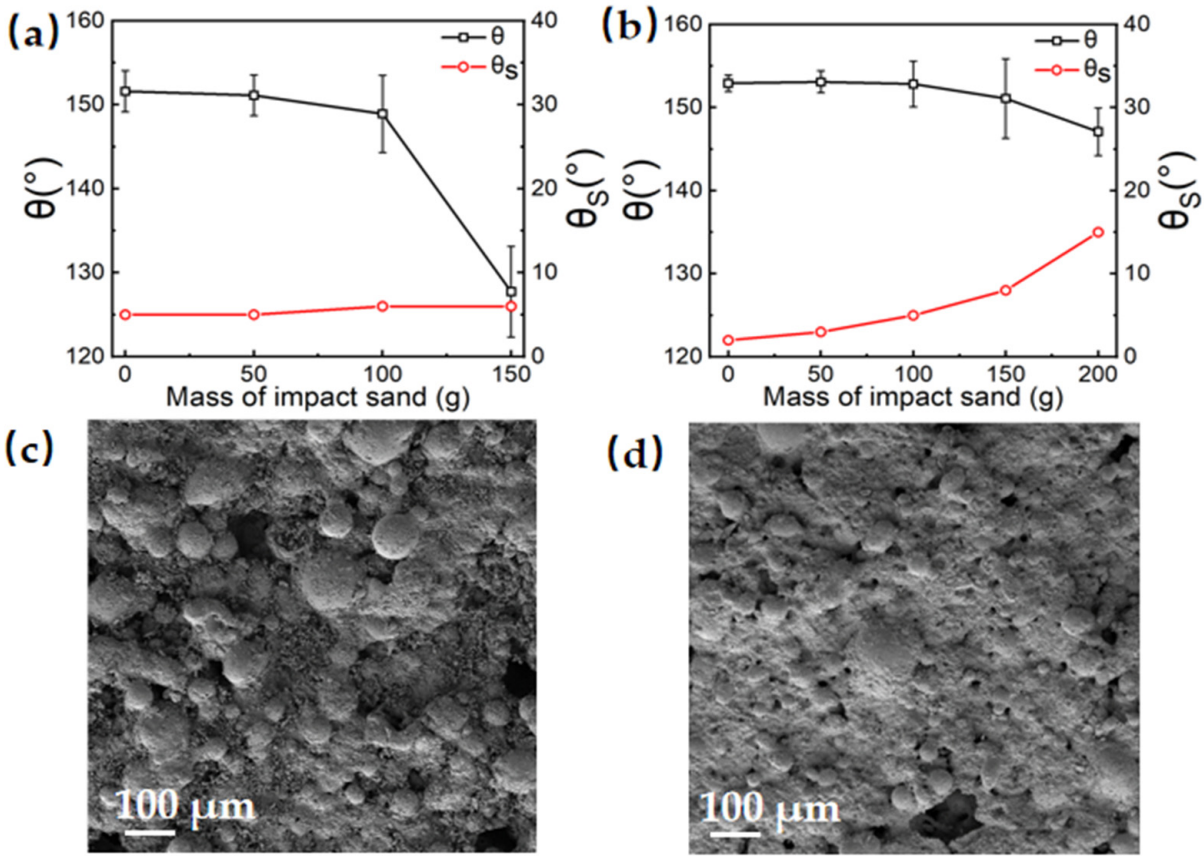

Figure 8. Sand impact test results for the (**a**) C10 sample and (**b**) C20 sample; the microscopic morphology of the (**c**) C10 and (**d**) C20 samples, respectively.

To evaluate the chemical durability of the coating, an immersion method was utilized to assess the performance of the C20 coating under strong acidic and alkaline conditions. Hydrochloric acid, with a concentration of 1 mol/L, and sodium hydroxide solution, with a concentration of 1 mol/L, were chosen to test the chemical durability of the coating. The test results are shown in Figure 9a,b. The durability of the C20 coating under acidic conditions significantly surpassed that under alkaline conditions. The hydrophobic angle merely dropped to 150° after two hours of immersion, whereas the superhydrophobicity of C20 was lost within half an hour under alkaline environments, and the hydrophobic angle rose to 45° under alkaline conditions. By analyzing the SEM images, as shown in Figure 9c,d, it can be seen that the surface of the C20 coating after strong acid immersion is slightly corroded, but it still displays a rough columnar structure, so the performance degradation is not obvious. However, after strong alkali immersion, the surface of C20 is corroded, and it loses its columnar structure, rapidly forfeiting its superhydrophobic properties. This is mainly because nano-Al_2O_3 can easily react with highly concentrated sodium hydroxide solutions, with a chemical mechanism of $Al_2O_3 + 2NaOH = 2NaAlO_2 + H_2O$. The product is soluble in water, thus triggering the loss of superhydrophobicity.

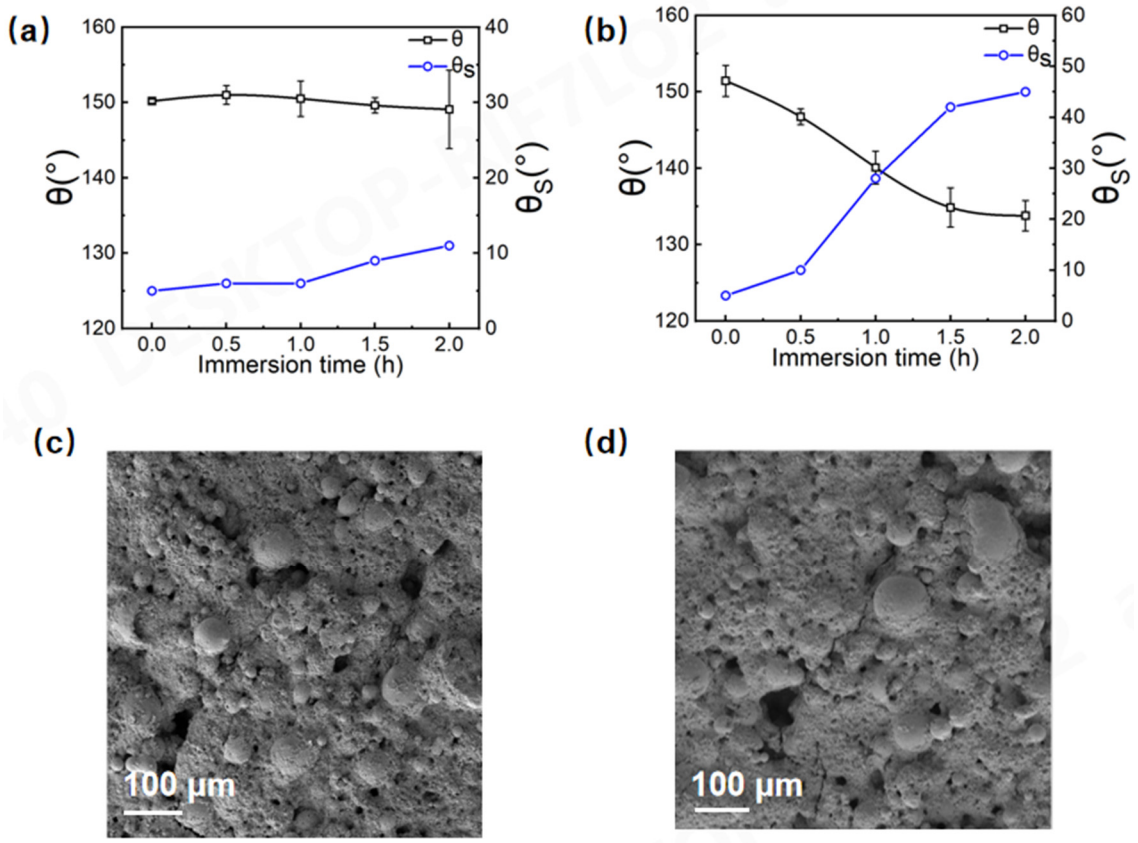

Figure 9. Results of chemical durability tests: (**a**) immersion in hydrochloric acid solution; (**b**) immersion in sodium hydroxide solution. Microscopic morphology of the coating surface after chemical durability testing via: (**c**) immersion in hydrochloric acid solution; (**d**) immersion in sodium hydroxide solution.

4. Conclusions

In summary, a robust superhydrophobic coating consisting of hydrophobic and rough micro/nano particles, along with additional NPs, was presented. The hydrophobic particles with various sizes construct the framework of the coating, and the additional nano-Al_2O_3 provides necessary nanoscale structures during abrasion. Compared with the sample prepared using only NPs and the NPs content of 10 wt.%, the surface with 20 wt.% NPs exhibited the best performance, withstanding 30 tape peeling tests, a 2.47 m sandpaper rubbing test (at a pressure of 5 kPa), the impact of 200 g of grit dropped from a height of 20 cm, and a 2 h acidic immersion. The coating also exhibited a high adhesion strength with the substrate, earning a grade assessment of 4B, while the surface prepared with only NPs and resin ranked the lowest, earning a grade of 0B. The results indicate that the inclusion of NPs is pivotal for retaining superhydrophobicity, while the hydrophobic particles prepared in this paper can protect nanoscale structures to increase their robustness. This simply fabricated coating will provide researchers with new paths for designing robust superhydrophobic coatings for large-scale indoor and outdoor applications.

Author Contributions: Conceptualization, L.S.; methodology, Y.L. and S.Y.; writing—original draft preparation, T.F. and Y.L.; formal analysis, T.F, Y.L., S.Y. and B.W.; writing—review and editing, T.F. and B.W.; supervision: L.S. and L.H. All authors have read and agreed to the published version of the manuscript.

Funding: This research was funded by the China Postdoctoral Foundation (2023M734307) and the 2023 Central Government Guides Local Science and Technology Development projects (2023ZYD0134).

Institutional Review Board Statement: Not applicable.

Informed Consent Statement: Not applicable.

Data Availability Statement: Data are contained within the article.

Conflicts of Interest: Author Tianyi Feng is employed by the company Avic General Huanan Aircraft Industry Co., Ltd. The remaining authors declare that the research was conducted in the absence of any commercial or financial relationships that could be construed as a potential conflict of interest.

References

1. Dalawai, S.P.; Aly, M.A.S.; Latthe, S.S.; Xing, R.; Sutar, R.S.; Nagappan, S.; Ha, C.-S.; Sadasivuni, K.K.; Liu, S. Recent advances in durability of superhydrophobic self-cleaning technology: A critical review. *Prog. Org. Coat.* **2020**, *138*, 105381. [CrossRef]
2. Liu, X.; Wang, P.; Zhang, D. Facile fabrication of high-aspect-ratio super-hydrophobic surface with self-propelled droplet jumping behavior for atmospheric corrosion protection. *Appl. Surf. Sci.* **2021**, *555*, 149549. [CrossRef]
3. Yang, Y.; Li, X.; Zheng, X.; Chen, Z.; Zhou, Q.; Chen, Y. 3D-printed biomimetic super-hydrophobic structure for microdroplet manipulation and oil/water separation. *Adv. Mater.* **2018**, *30*, 1704912. [CrossRef] [PubMed]
4. Su, Y.; Zhao, Y.; Zheng, W.; Yu, H.; Liu, Y.; Xu, L. Asymmetric Sc-PLA membrane with multi-scale microstructures: Wettability, antifouling, and oil–water separation. *ACS Appl. Mater. Interfaces* **2020**, *12*, 55520–55526. [CrossRef] [PubMed]
5. Yu, H.; Wu, M.; Duan, G.; Gong, X. One-step fabrication of eco-friendly superhydrophobic fabrics for high-efficiency oil/water separation and oil spill cleanup. *Nanoscale* **2022**, *14*, 1296–1309. [CrossRef]
6. Ye, Y.; Zhang, D.; Li, J.; Liu, T.; Pu, J.; Zhao, H.; Wang, L. One-step synthesis of superhydrophobic polyhedral oligomeric silsesquioxane-graphene oxide and its application in anti-corrosion and anti-wear fields. *Corros. Sci.* **2019**, *147*, 9–21. [CrossRef]
7. Li, D.-W.; Wang, H.-Y.; Liu, Y.; Wei, D.-S.; Zhao, Z.-X. Large-scale fabrication of durable and robust super-hydrophobic spray coatings with excellent repairable and anti-corrosion performance. *Chem. Eng. J.* **2019**, *367*, 169–179. [CrossRef]
8. Wei, J.; Li, B.; Jing, L.; Tian, N.; Zhao, X.; Zhang, J. Efficient protection of Mg alloy enabled by combination of a conventional anti-corrosion coating and a superamphiphobic coating. *Chem. Eng. J.* **2020**, *390*, 124562. [CrossRef]
9. Hu, J.; Jiang, G. Superhydrophobic coatings on iodine doped substrate with photothermal deicing and passive anti-icing properties. *Surf. Coat. Technol.* **2020**, *402*, 126342. [CrossRef]
10. Latthe, S.S.; Sutar, R.S.; Kodag, V.S.; Bhosale, A.; Kumar, A.M.; Sadasivuni, K.K.; Xing, R.; Liu, S. Self–cleaning superhydrophobic coatings: Potential industrial applications. *Prog. Org. Coat.* **2019**, *128*, 52–58. [CrossRef]
11. Wang, N.; Wang, Q.; Xu, S. A review on applications of superhydrophobic materials in civil engineering. *Adv. Eng. Mater.* **2022**, *24*, 2101238. [CrossRef]
12. Yang, Y.; Bian, Y.; Gao, Q.; Dong, S.; Ma, R.; Fan, Y.; Du, A.; Zhao, X.; Yang, M.; Cao, X. Corrosion resistance study of Zn-Ni-B4C composite superhydrophobic coatings with hierarchical rough structure. *Appl. Surf. Sci.* **2023**, *622*, 156882. [CrossRef]
13. Malavasi, I.; Bernagozzi, I.; Antonini, C.; Marengo, M. Assessing durability of superhydrophobic surfaces. *Surf. Innov.* **2015**, *3*, 49–60. [CrossRef]
14. Chang, Z.; Lu, Y. Fabrication of superhydrophobic surfaces with Cassie-Baxter state. *J. Dispers. Sci. Technol.* **2022**, *43*, 1099–1111. [CrossRef]
15. Liu, Z.; Zhang, C.; Jing, J.; Zhang, X.; Wang, C.; Liu, F.; Jiang, M.; Wang, H. Bristle worm inspired ultra-durable superhydrophobic coating with repairable microstructures and anti-corrosion/scaling properties. *Chem. Eng. J.* **2022**, *436*, 135273. [CrossRef]
16. Liu, D.; Liu, J.; Liu, G.; Xie, Y.; Duan, Z. Study on corrosion resistance of LDH/micro-arc oxidation composite superhydrophobic coatings on AZ31 magnesium alloy. *Coatings* **2023**, *13*, 643. [CrossRef]
17. Hassan, N.; Fadhali, M.M.; Al-Sulaimi, S.; Al-Buriahi, M.; Katubi, K.M.; Alrowaili, Z.; Khan, M.A.; Shoukat, R.; Ajmal, Z.; Abbas, F. Development of sustainable superhydrophobic coatings on aluminum substrate using magnesium nanoparticles for enhanced catalytic activity, self-cleaning, and corrosion resistance. *J. Mol. Liq.* **2023**, *383*, 122085. [CrossRef]
18. Chen, W.; Shi, H.; Liu, W.; Zhao, A.; Pan, G.; Huang, A.; Yu, Y.; Ma, L. Study on the preparation and corrosion resistance properties of superhydrophobic coatings on galvanized steel. *Metals* **2023**, *13*, 260. [CrossRef]
19. Gao, M.; Li, Y.; Su, X.; Tang, Z.; Han, Z.; Zhang, Z.; Chai, W.; Zhang, W.; Zheng, Z.; Liu, Y. One-step spraying route to construct a bio-inspired, robust, multi-functional and superhydrophobic coatings with corrosion resistance, self-cleaning and anti-icing properties. *Colloids Surf. A Physicochem. Eng. Asp.* **2023**, *676*, 132225. [CrossRef]
20. Wu, Q.; Xu, J.; Tu, N.; Xue, B.; Chen, J.; Lu, H. Preparation of mechanically durable superhydrophobic aluminum surfaces by LST/MAO and chemical modification. *Colloids Surf. A Physicochem. Eng. Asp.* **2024**, *689*, 133722. [CrossRef]
21. Zhang, Z.; Xue, F.; Bai, W.; Shi, X.; Liu, Y.; Feng, L. Superhydrophobic surface on Al alloy with robust durability and excellent self-healing performance. *Surf. Coat. Technol.* **2021**, *410*, 126952. [CrossRef]
22. Verro, V.; Di Franco, F.; Zaffora, A.; Santamaria, M. Enhancing corrosion resistance of anodized AA7075 alloys by electrodeposition of superhydrophobic coatings. *Colloids Surf. A Physicochem. Eng. Asp.* **2023**, *675*, 132040. [CrossRef]
23. Xu, J.; Wang, G.; Li, J.; Li, Y.; Cai, Q.; Lian, Z.; Yu, H. Antireflection Property and Corrosion Resistance of Black Ceramic Superhydrophobic Coatings on Aluminum Alloy. *Adv. Eng. Mater.* **2024**, *26*, 2301507. [CrossRef]
24. Cassie, A.; Baxter, S. Wettability of porous surfaces. *Trans. Faraday Soc.* **1944**, *40*, 546–551. [CrossRef]
25. Sun, R.; Jin, B.; Yao, L.; Liu, Y.; Li, J.; Liang, J.; He, J. Controllable design of bifunctional VO_2 coatings with superhydrophobic and thermochromic performances. *ACS Appl. Mater. Interfaces* **2021**, *13*, 13751–13759. [CrossRef]

26. Zhang, X.; Zhang, H.; Cheng, Y.; Zhang, L.; Shen, W. Superhydrophobic surfaces with dual-scale roughness and water vapor-barrier property for sustainable liquid packaging applications. *Cellulose* **2022**, *29*, 9777–9790. [CrossRef]
27. Fan, S.; Li, L.; Sun, K.; Zhang, T.; Wang, L.; Wang, Z. Fabrication of Superhydrophobic Hierarchical Structures on PET Surfaces by Hot Embossing with in Situ Growth of Silver Nanoparticles. In Proceedings of the 2023 IEEE International Conference on Manipulation, Manufacturing and Measurement on the Nanoscale (3M-NANO), Chengdu, China, 31 July–4 August 2023; pp. 327–330.
28. Kang, H.H.; Lee, D.H. Facile preparation of superhydrophobic nanorod surfaces through ion-beam irradiation. *Surf. Interface Anal.* **2022**, *54*, 813–819. [CrossRef]
29. Wang, P.; Li, C.; Zhang, D. Recent advances in chemical durability and mechanical stability of superhydrophobic materials: Multi-strategy design and strengthening. *J. Mater. Sci. Technol.* **2022**, *129*, 40–69. [CrossRef]
30. Nyankson, E.; Agbe, H.; Takyi, G.K.S.; Bensah, Y.D.; Sarkar, D.K. Recent advances in nanostructured superhydrophobic surfaces: Fabrication and long-term durability challenges. *Curr. Opin. Chem. Eng.* **2022**, *36*, 100790. [CrossRef]
31. Celik, N.; Akay, S.; Sahin, F.; Sezer, G.; Dagasan Bulucu, E.; Ruzi, M.; Butt, H.J.; Onses, M.S. Sustainable and practical superhydrophobic surfaces via mechanochemical grafting. *Adv. Mater. Interfaces* **2023**, *10*, 2300069. [CrossRef]
32. Li, L.; Wei, J.; Zhang, J.; Li, B.; Yang, Y.; Zhang, J. Challenges and strategies for commercialization and widespread practical applications of superhydrophobic surfaces. *Sci. Adv.* **2023**, *9*, eadj1554. [CrossRef]
33. Huang, Z.-S.; Quan, Y.-Y.; Mao, J.-J.; Wang, Y.-L.; Lai, Y.; Zheng, J.; Chen, Z.; Wei, K.; Li, H. Multifunctional superhydrophobic composite materials with remarkable mechanochemical robustness, stain repellency, oil-water separation and sound-absorption properties. *Chem. Eng. J.* **2019**, *358*, 1610–1619. [CrossRef]
34. Bai, Z.; Zhang, B. Fabrication of superhydrophobic reduced-graphene oxide/nickel coating with mechanical durability, self-cleaning and anticorrosion performance. *Nano Mater. Sci.* **2020**, *2*, 151–158. [CrossRef]
35. Yu, X.; Shi, X.; Xue, F.; Bai, W.; Li, Y.; Liu, Y.; Feng, L. SiO_2 nanoparticle-containing superhydrophobic materials with enhanced durability via facile and scalable spray method. *Colloids Surf. A Physicochem. Eng. Asp.* **2021**, *626*, 127014. [CrossRef]
36. He, P.; Qu, J.; Li, S.; Sun, R.; Huang, K.; Zhao, J.; Mo, J. Study on the construction of durable superhydrophobic coatings using simple spray coating method and their underwater drag reduction performance. *Colloids Surf. A Physicochem. Eng. Asp.* **2024**, *701*, 134858. [CrossRef]
37. Li, W.; Wang, Y.; Feng, Y.; Wang, Q.; Xu, X.; Li, G.; Dong, G.; Jing, S.; Chen, E.; Fan, X. Fabrication of robust conductive and superhydrophobic coating based on carbon nanotubes. *Mater. Res. Express* **2020**, *7*, 055009. [CrossRef]
38. Xu, S.; Wang, Q.; Wang, N. Chemical fabrication strategies for achieving bioinspired superhydrophobic surfaces with micro and nanostructures: A review. *Adv. Eng. Mater.* **2021**, *23*, 2001083. [CrossRef]
39. Selim, M.S.; Fatthallah, N.A.; Shenashen, M.A.; Higazy, S.A.; Madian, H.R.; Selim, M.M.; El-Safty, S.A. Bioinspired graphene oxide–magnetite nanocomposite coatings as protective superhydrophobic antifouling surfaces. *Langmuir* **2023**, *39*, 2333–2346. [CrossRef] [PubMed]
40. Ma, Y.; Wei, J.; Cai, Y.; Zheng, J.; Bittencourt, C.; Fan, H. Facile fabrication of self-roughened surfaces for superhydrophobic coatings via polarity-induced phase separation strategy. *J. Colloid Interface Sci.* **2022**, *628*, 777–787. [CrossRef]
41. Arcot, Y.; Liu, S.; Ulugun, B.; DeFlorio, W.; Bae, M.; Salazar, K.S.; Taylor, T.M.; Castillo, A.; Cisneros-Zevallos, L.; Scholar, E.M. Fabrication of robust superhydrophobic coatings onto high-density polyethylene food contact surfaces for enhanced microbiological food safety. *ACS Food Sci. Technol.* **2021**, *1*, 1180–1189. [CrossRef]
42. Liu, M.; Luo, Y.; Jia, D. Polydimethylsiloxane-based superhydrophobic membranes: Fabrication, durability, repairability, and applications. *Polym. Chem.* **2020**, *11*, 2370–2380. [CrossRef]
43. Bayer, I.S. Superhydrophobic coatings from ecofriendly materials and processes: A review. *Adv. Mater. Interfaces* **2020**, *7*, 2000095. [CrossRef]
44. Zhao, Y.; Wen, K.; Wang, J.; Yang, Z.; Qin, M. Preparation, characterisation, and anti-icing properties of superhydrophobic coatings on asphalt mixture. *Int. J. Pavement Eng.* **2023**, *24*, 2118271. [CrossRef]
45. Li, J.; Yu, F.; Jiang, Y.; Wang, L.; Liu, Y.; Yang, X.; Li, X.; Lü, W. Superhydrophobic coating with a micro-and nano-sized MnO_2/PDMS composite structure for passive anti-icing/active de-icing and photothermal applications. *J. Mater. Chem. C* **2023**, *11*, 15443–15453. [CrossRef]
46. Fan, T.; Zhao, Q.; Guo, W.; Mao, H.; He, B.; Ruan, W. Effects of inorganic particles on the crystallization, mechanical properties and cellular structure of foamed PP composites in the IMD/MIM process. *RSC Adv.* **2021**, *11*, 36651–36662. [CrossRef]
47. Huang, X.; Yu, R. Robust superhydrophobic and repellent coatings based on micro/nano SiO_2 and fluorinated epoxy. *Coatings* **2021**, *11*, 663. [CrossRef]
48. Bao, J.; He, J.; Chen, B.; Yang, H.; Jie, J.; Wang, R.; Zhang, S. Multi-scale superhydrophobic anti-icing coating for wind turbine blades. *Energy Eng.* **2021**, *118*, 947–959. [CrossRef]
49. Zhang, F.; Xu, D.; Ma, L.; Wang, J.; Chen, H.; Guo, S. Preparation and properties of modified SiO_2/epoxy resin superhydrophobic coating. *Surf. Topogr. Metrol. Prop.* **2024**, *12*, 035005. [CrossRef]
50. Chen, A.; Zhao, Y.; Chen, H.; Ma, H.; Lv, K. Facile design of PTFE-kaolin-based ternary nanocomposite as a hydrophobic and high corrosion-barrier coating. *Rev. Adv. Mater. Sci.* **2024**, *63*, 20240019. [CrossRef]
51. Gu, W.; Li, W.; Zhang, Y.; Xia, Y.; Wang, Q.; Wang, W.; Liu, P.; Yu, X.; He, H.; Liang, C. Ultra-durable superhydrophobic cellular coatings. *Nat. Commun.* **2023**, *14*, 5953. [CrossRef]

52. Celik, N.; Sahin, F.; Ozel, S.S.; Sezer, G.; Gunaltay, N.; Ruzi, M.; Onses, M.S. Self-healing of biocompatible superhydrophobic coatings: The interplay of the size and loading of particles. *Langmuir* **2023**, *39*, 3194–3203. [CrossRef] [PubMed]
53. Guo, X.-J.; Zhang, D.; Xue, C.-H.; Liu, B.-Y.; Huang, M.-C.; Wang, H.-D.; Wang, X.; Deng, F.-Q.; Pu, Y.-P.; An, Q.-F. Scalable and mechanically durable superhydrophobic coating of SiO_2/polydimethylsiloxane/epoxy nanocomposite. *ACS Appl. Mater. Interfaces* **2023**, *15*, 4612–4622. [CrossRef] [PubMed]
54. Ke, C.; Fang, Y.; Zhou, Z.; Wang, G.; Liu, Y.; Wu, W.; Xiao, L.; Zhang, M.; Hu, H.; Liu, J. Superhydrophobic composite coating with excellent mechanical durability. *Coatings* **2022**, *12*, 185. [CrossRef]
55. Binrui, W.; Qiong, Q.; Xuan, J.; Dong, X.; Liping, S.; Xin, C.; Qizhi, Z.; Feiyan, F.; Xian, Y. A highly robust, concrete-inspired superhydrophobic nanocomposite coating. *Nanoscale* **2023**, *15*, 19304–19313. [CrossRef]
56. Wang, Y.; Huang, J.-T. Large-Scale Fabrication of Graded Convex Structure for Superhydrophobic Coating Inspired by Nature. *Materials* **2022**, *15*, 2179. [CrossRef]
57. Xia, R.; Zhang, B.; Dong, K.; Yan, Y.; Guan, Z. HD-SiO_2/SiO_2 Sol@ PDMS superhydrophobic coating with good durability and anti-corrosion for protection of Al sheets. *Materials* **2023**, *16*, 3532. [CrossRef]
58. *ASTM D3359-23*; Standard Test Methods for Rating Adhesion by Tape Test. ASTM: West Conshohocken, PA, USA, 2023. [CrossRef]